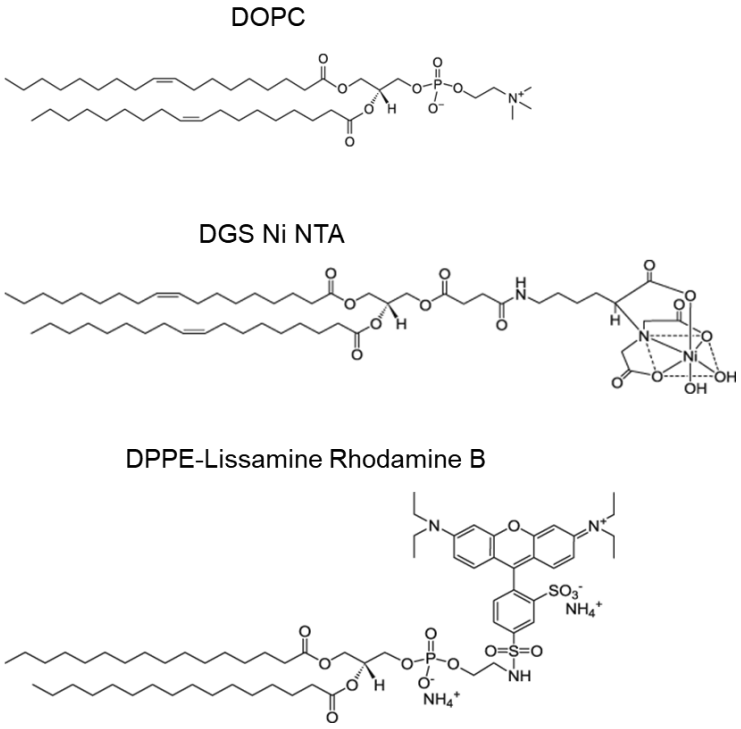

Figure S1. Lipid structures: 1,2-dioleoyl-sn-glycero-3-phosphocholine (DOPC), 1,2-dioleoyl-sn-glycero-3-[(N-(5-amino-1-carboxypentyl)iminodiacetic acid)succinyl] (nickel salt) (DGS NTA (Ni)), 1,2-dipalmitoyl-sn-glycero-3-phosphoethanolamine-N-(lissamine rhodamine B sulfonyl) (ammonium salt) (Liss Rhod PE).

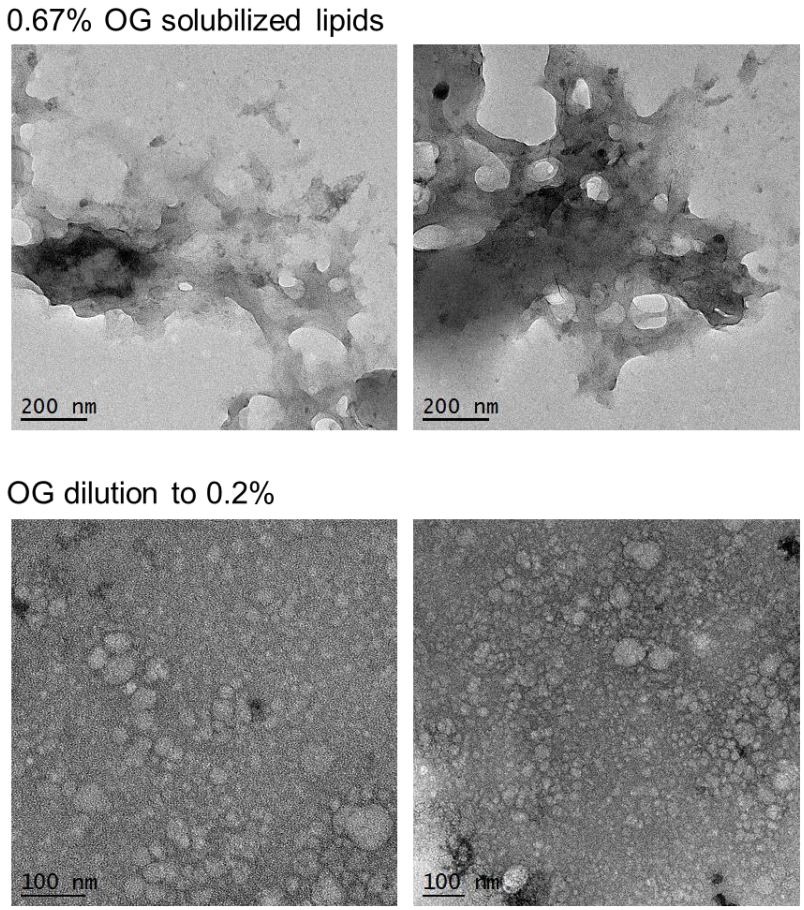

Figure S2. Negative stained TEM images of 0.67% OG-solubilized lipids (top) and lipids with subsequently diluted OG to 0.2% (bottom). Scale bars included.

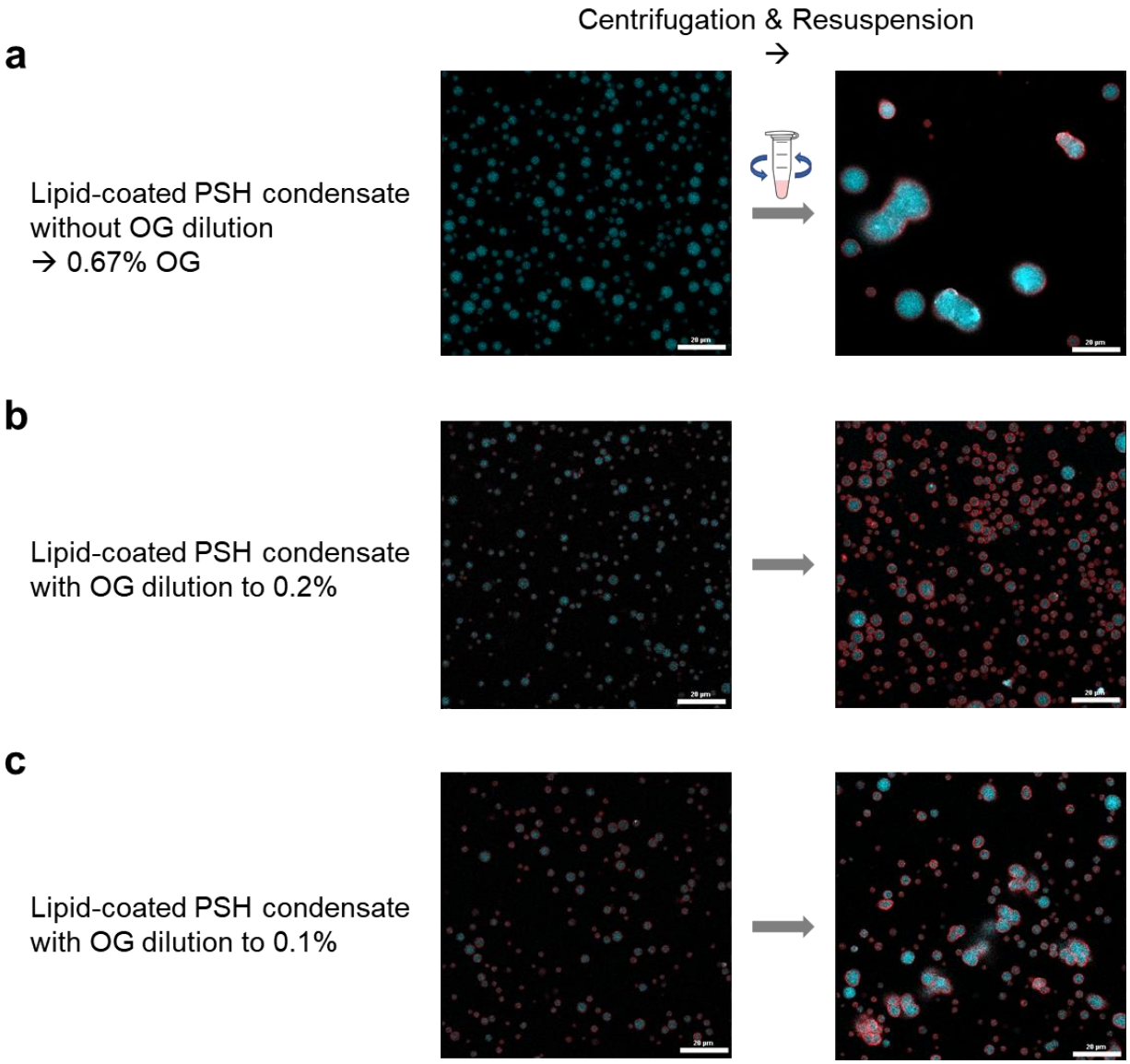

Figure S3. Confocal images of lipid-coated PSH condensates before (left) and after (right) centrifugation with different OG concentrations. (a) PSH condensates were mixed with OG solubilized lipids (final OG concentration 0.67%) and centrifuged/resuspended without further OG dilution. (b, c) PSH condensates were mixed with OG solubilized lipids (final OG concentration 0.67%) and diluted to (b) 0.2% OG or to (c) 0.1% OG, followed by centrifugation/resuspension. Scale bars 20 μm.

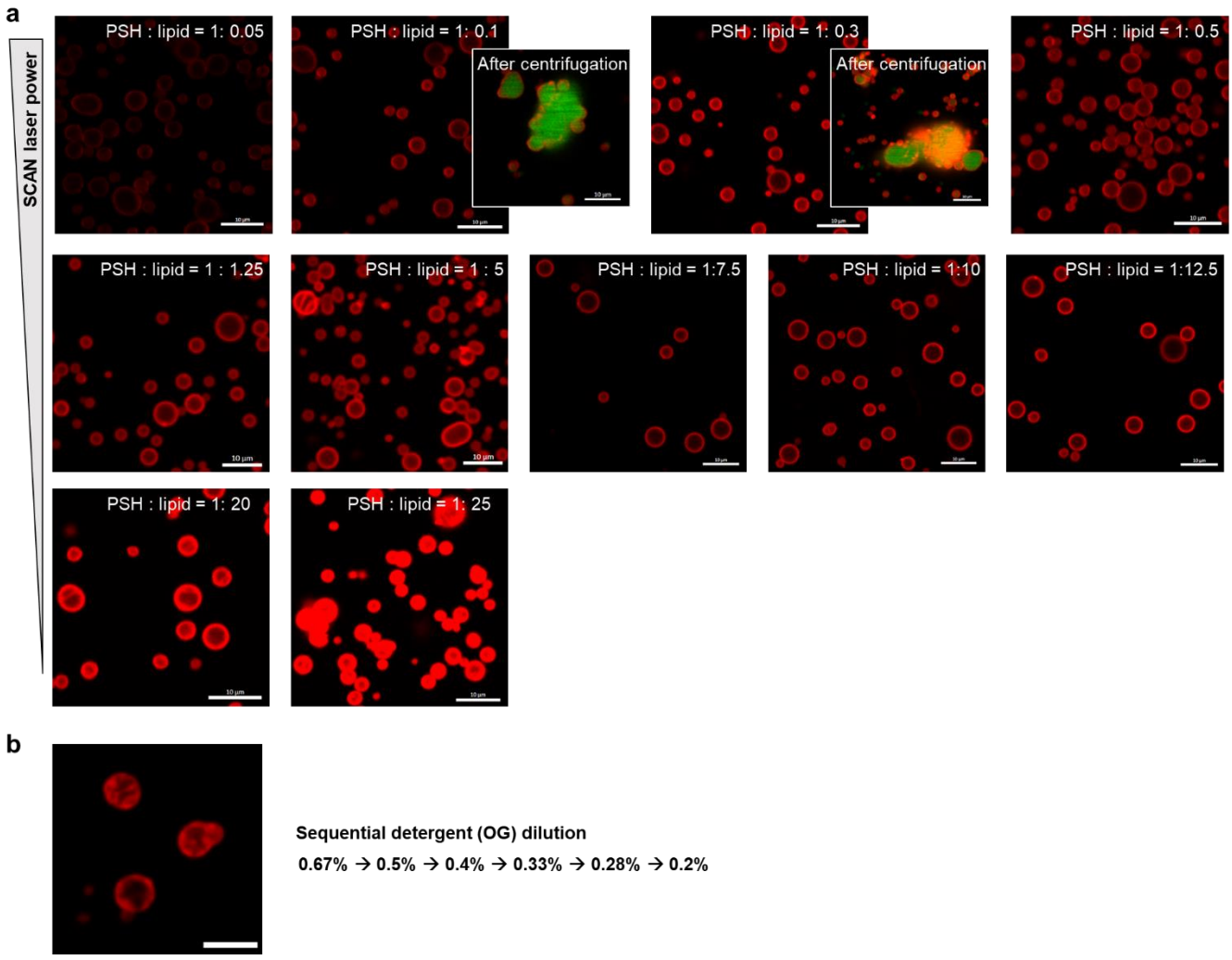

Figure S4. Lipid coating changes by protein:lipid ratios. (a) Confocal images of lipid-coated PSH condensates at varying PSH:lipid ratios (final molar concentration). An image scan excitation power was increased for low lipid samples. Protocell aggregation images after centrifugation are shown for PSH:lipid 1:0.1 and 1:0.3 samples. (b) Confocal image of lipid-coated PSH condensates prepared by sequential OG dilution rather than rapid dilution from 0.67% to 0.2%. Scale bars 10 μm.

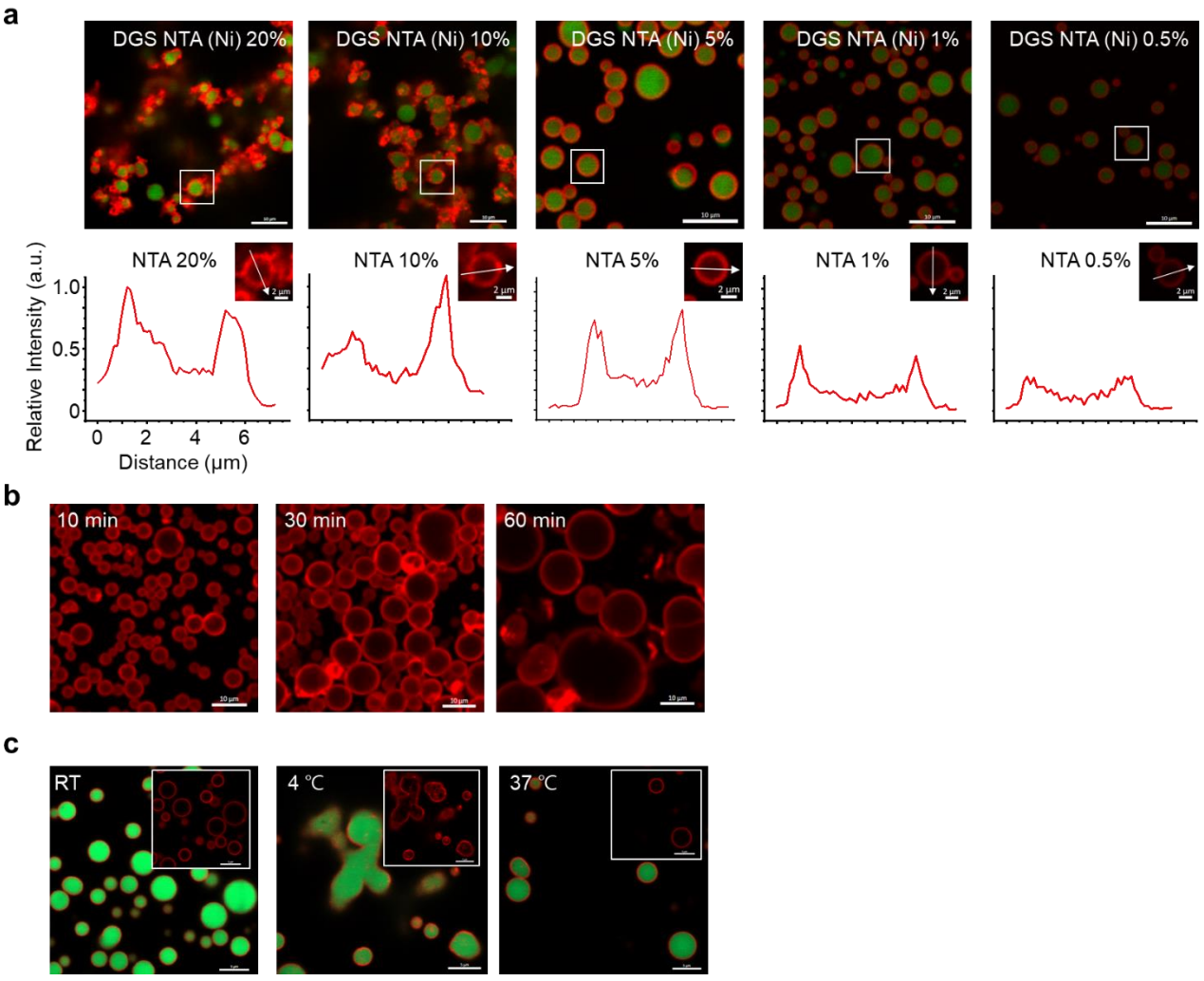

Figure S5. Lipid coating method variation. (a) Lipid coating with different DGS NTA (Ni) portions. The line scans of surface lipid intensities for boxed condensates were shown below. The same relative intensity and distance scales are applied for all scans. Scale bars 10 μm (2 μm for inserts). (b) Lipid coating at different PSH condensate formation time. Condensate formation was induced by metal addition, and the resulting mixtures were incubated for indicated time before lipid addition. (c) Lipid coating at different temperatures. Scale bars 10 μm (5 μm for inserts).

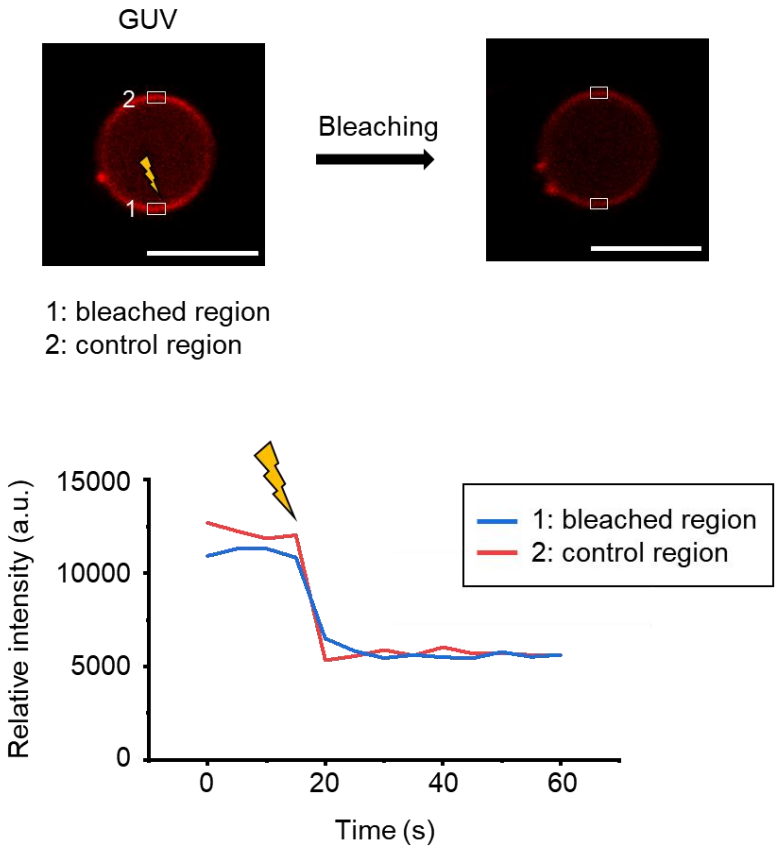

Figure S6. FRAP recovery profiles and images of GUV forming lipids. The bleached area of the lipid layer (1) and the control area without bleaching (2) are indicated with white boxes. Signals of both regions were rapidly decreased by bleaching, likely due to rapid lateral diffusion of GUV lipids. Scale bars 5 μm.

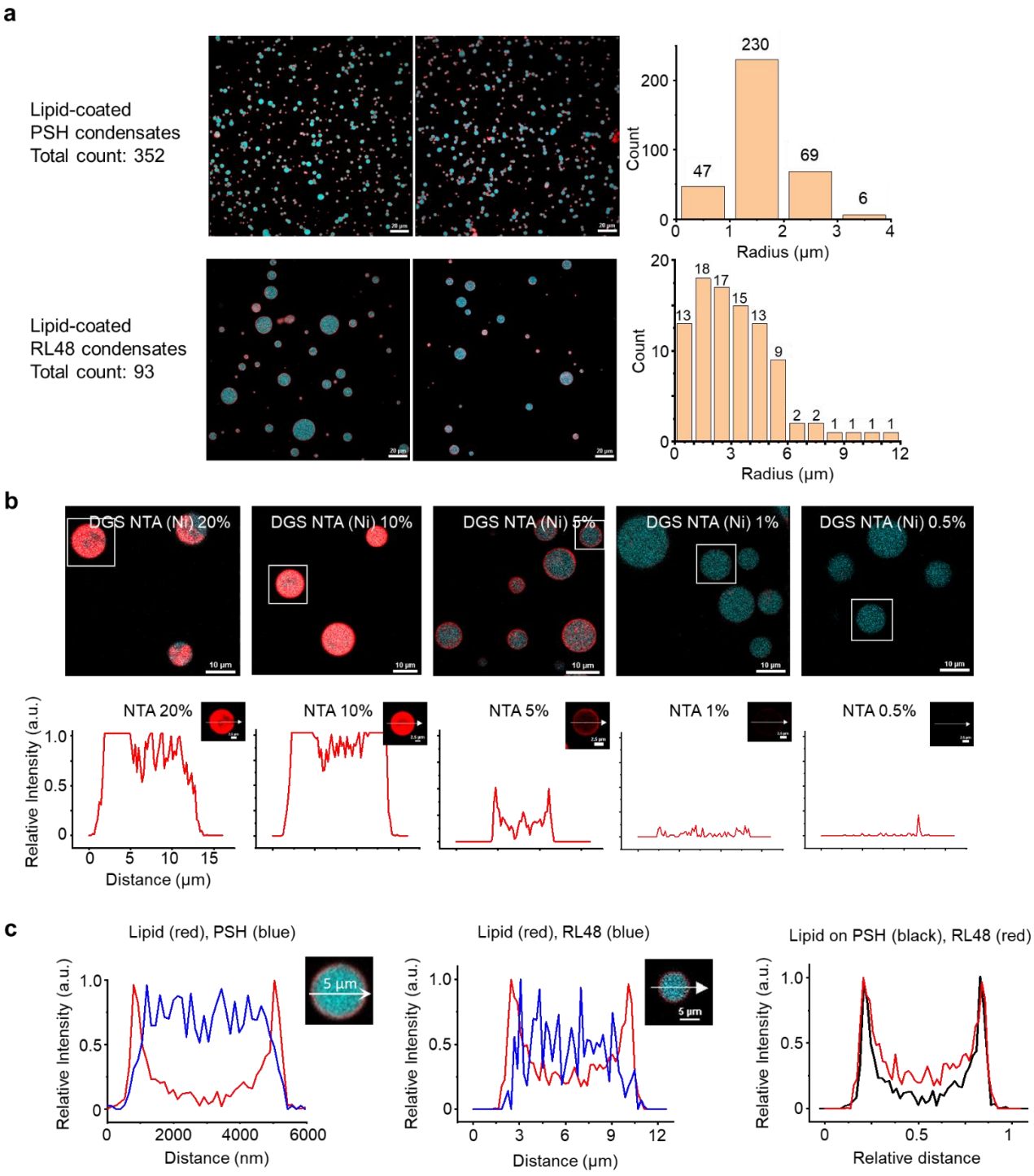

Figure S7. Lipid-coated RL48 condensate protocell formation. (a) Whole confocal images of PSH (top) and RL48 (bottom) protocells with size distribution profiles (right). 352 PSH and 93 RL48 well dispersed and circular form (circularity 0.7-1.0) protocells are examined. Scale bars 20 μm. (b) Confocal images of lipid-coated RL48 protocells with different DGS-NTA (Ni) portions. The line scans of surface lipid intensities for boxed condensates were shown below. The same relative intensity and distance scales are applied for all scans. Scale bars 10 μm (2 μm for inserts). (c) Fluorescence intensity profiles of lipids (red) and PSH/RL48 (cyan) across (white arrow) a lipid-coated PSH (left)

or RL48 (middle) condensate. PSH profiles are identical to Figure 1c. Lipid intensity profiles of PSH (black) and RL48 (red) condensates are also shown (right) for comparison. Scale bars 5 μm.

Note I: All examined protocells are well coated with lipids. Compare to PSH protocells, fewer but larger RL48 protocells were produced, and thereby fewer protocells were examined from the same number of whole confocal images.

Note II: With high NTA-lipid concentrations, a large portion of lipids penetrated into RL48 condensates (Figure S7b). Overlaid lipid intensity profiles for PSH and RL48 protocells also indicate more lipid penetration into RL48 condensates (Figure S7c, right).

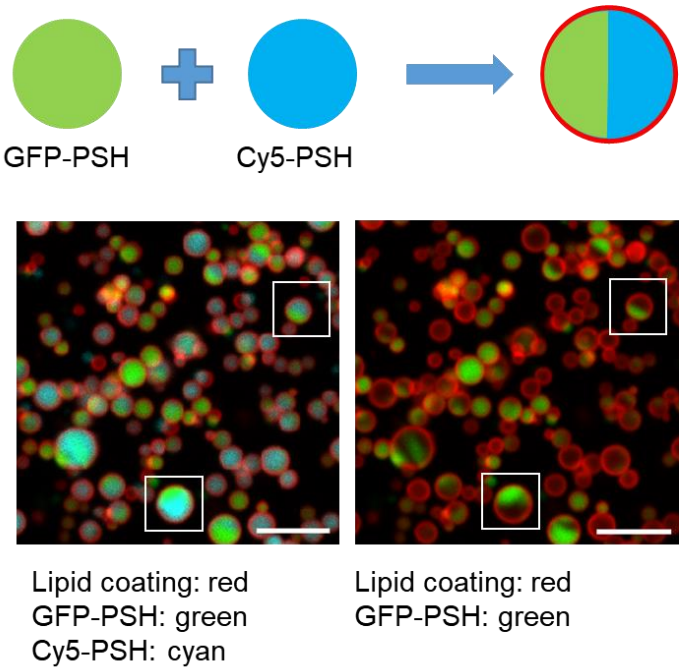

Figure S8. Lipid coating on heterogeneous PSH condensates. Differently labelled PSH condensates were separately formed, fused, and coated with lipids. Images are identical except Cy5-PSH signals (cyan). Scale bars 10 μm.

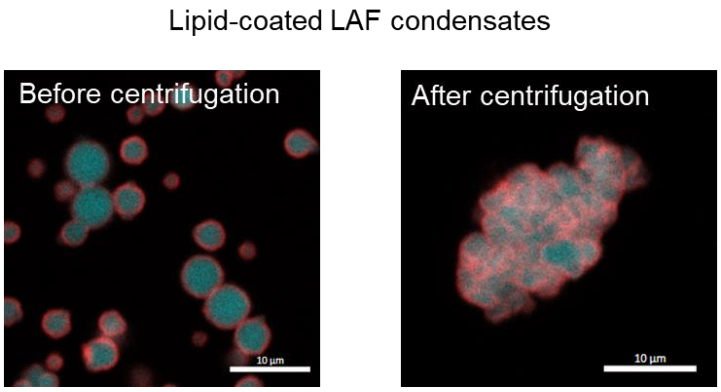

Figure S9. Lipid-coated protocell formation with intrinsically disordered LAF condensates. Scale bars 10 µm.

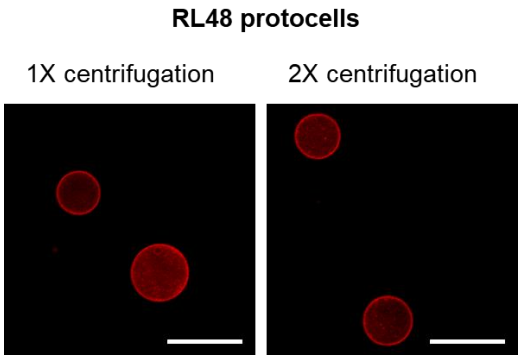

Figure S10. Confocal images of RL48 protocells after first (left) and second (right) centrifugation. Scale bars 20 μm.

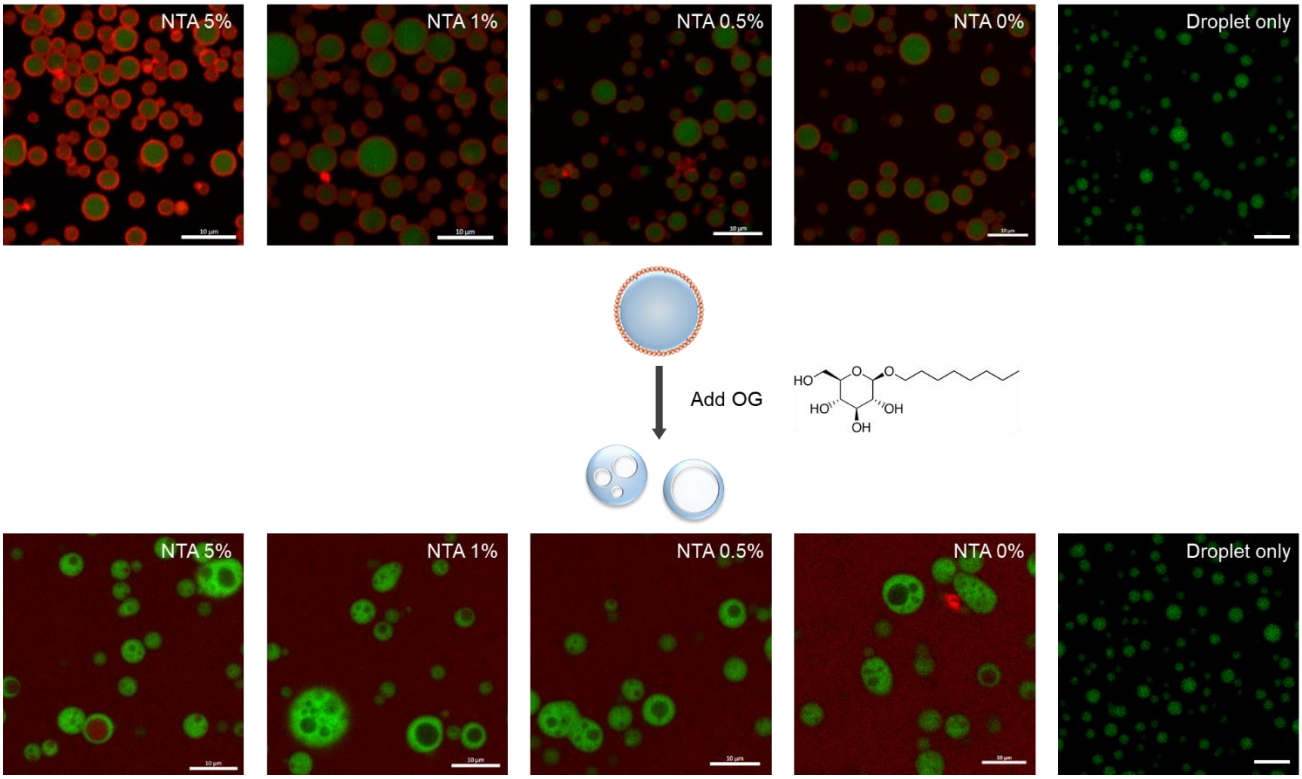

Figure S11. Confocal images of hollow cavity formation inside PSH protocells, which contain different DGS NTA ratios of lipid coating, by detergent (Octyl glucoside, OG) addition. Protein condensates without a lipid coating (Droplet only) are not affected by OG addition. Scale bars 10 μm.

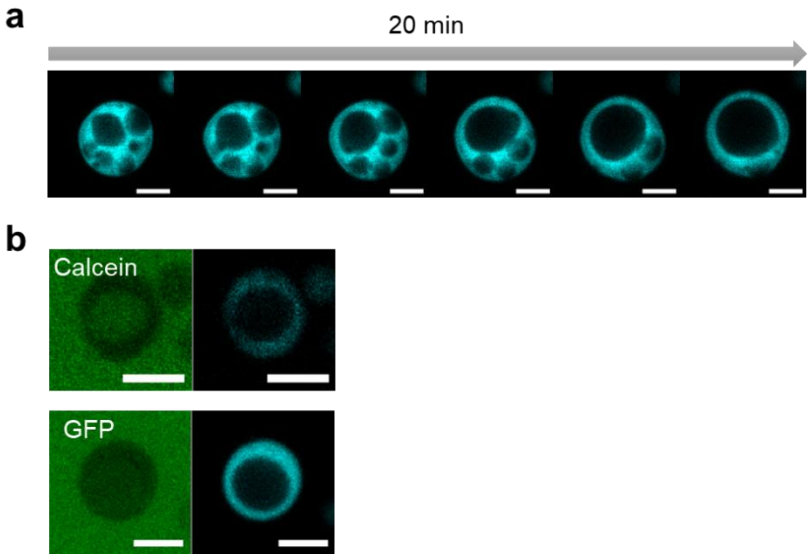

Figure S12. Properties of detergent-induced disruption of PSH condensate protocells. (a) Real-time images of cavity fusion inside a condensate over 20 min. (b) Inclusion of external materials (calcein and GFP) in lipid cavities. Scale bars 5 μm.

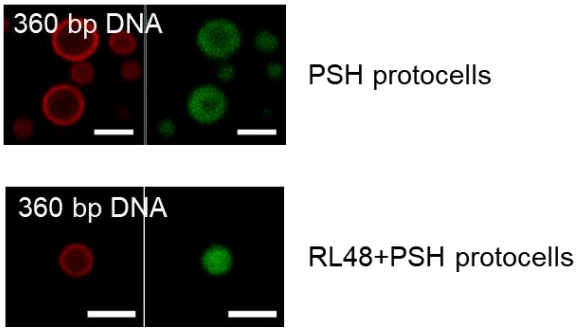

Figure S13. Permeability of PSH and RL48+PSH protocells against long DNA (360 bp). Scale bars 5 μm.

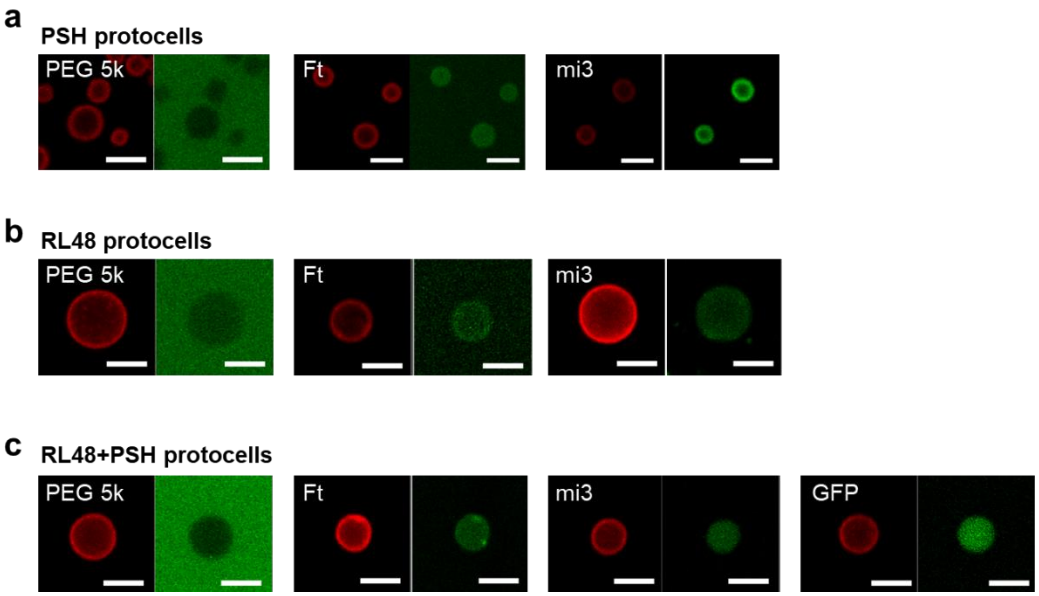

Figure S14. Permeability of PSH, RL48, and RL48+PSH protocells against PEG 5kDa, ferritin (Ft), and artificial cage mi3. Scale bars 5 μm.

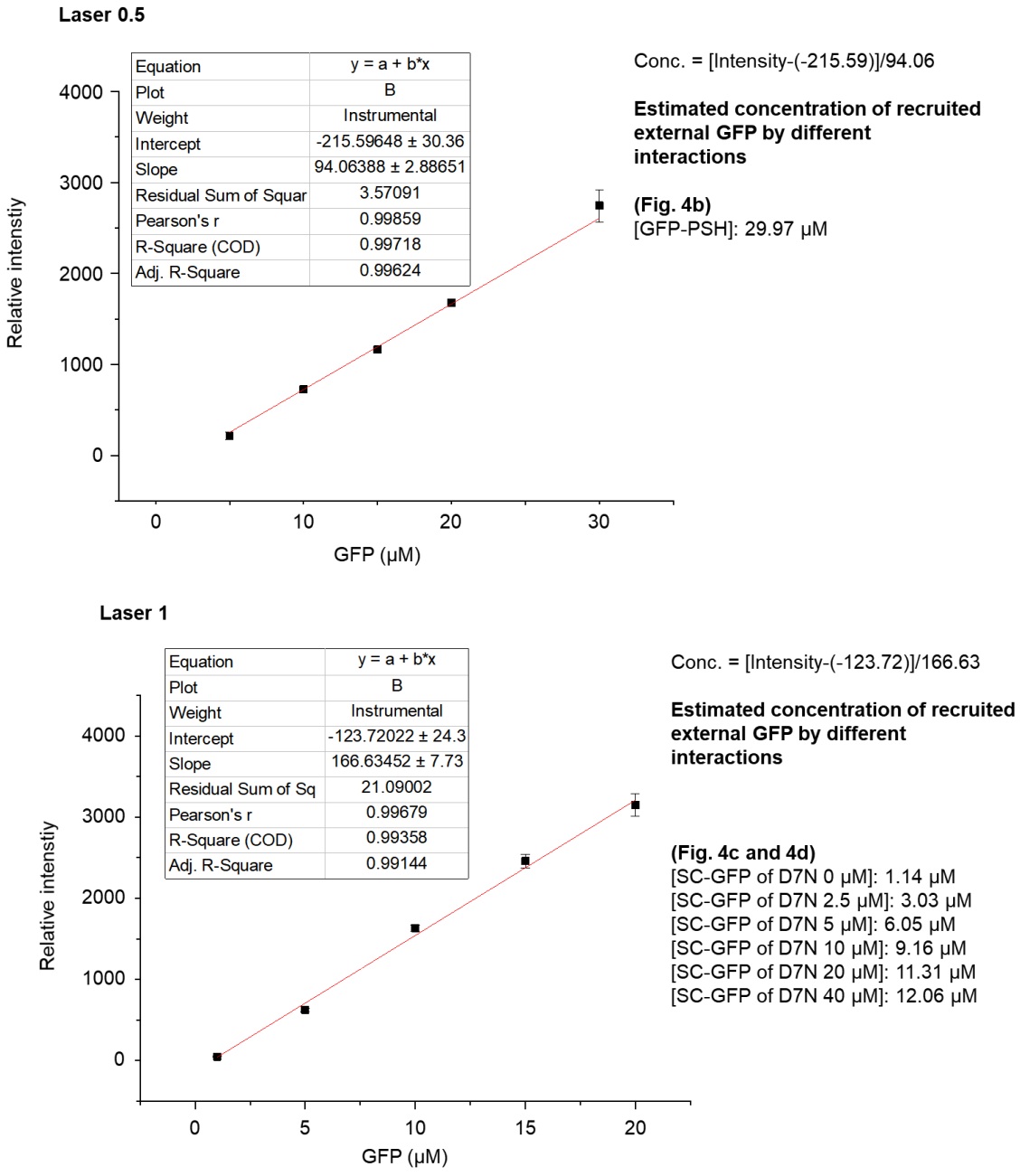

Figure S15. GFP signal calibration to quantify GFP concentrations inside protocells. Concentrations of recruited external GFP variants (Figures are indicated) are estimated in the right. Laser powers are adjusted based on inside GFP signal intensities.

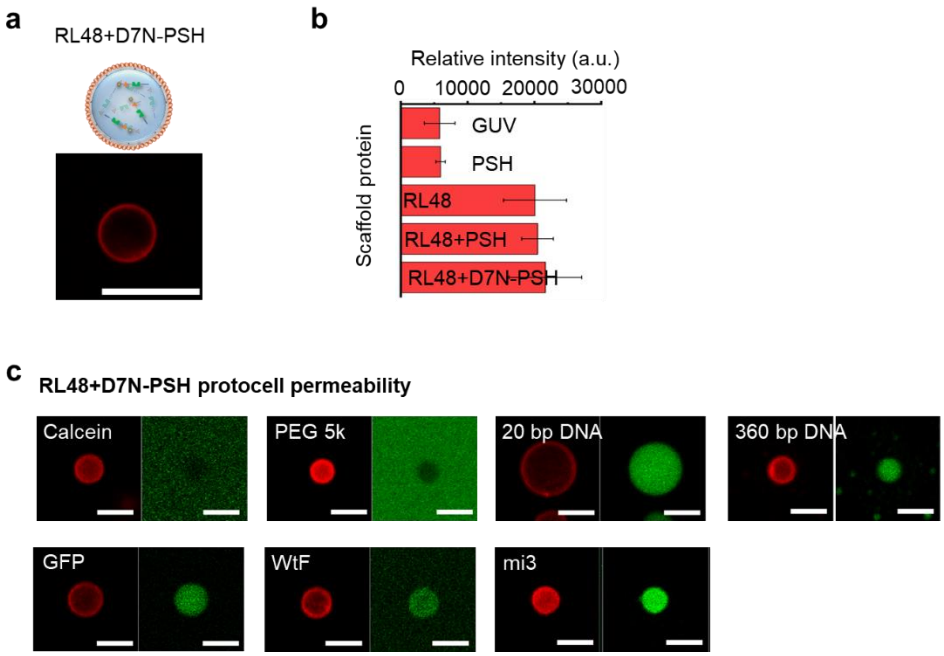

Figure S16. Properties of RL48+D7N-PSH condensate protocells. (a) Confocal image of a lipid-coated RL48+D7N-PSH condensate. Scale bar 10 μm. (b) Total fluorescent intensities of lipid coatings of GUV and protocells with different protein condensates. Error bars: 1 s. d. (n = 8). GUV and other protocell data are from Figure 1i. (c) Permeability of RL48+D7N-PSH protocells. Scale bars 5 μm.

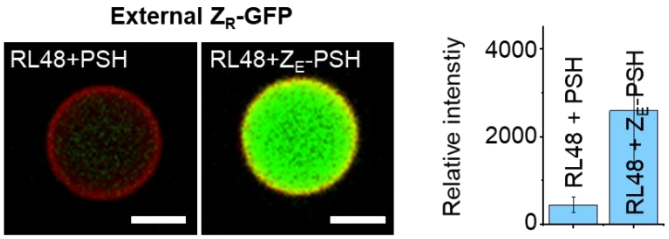

Figure S17. Confocal images of RL48+PSH (left) and RL48+Z_E-PSH (right) protocells treated with Z_R-GFP. Relative intensities of recruited GFP signals are shown in the right graph. Scale bars 5 μm. Error bars: 1 s. d. (n > 7). A strong lazer power was used for imaging due to relatively weak ZR-GFP recruitment, compared to GFP-PSH and SC-GFP recruitment.

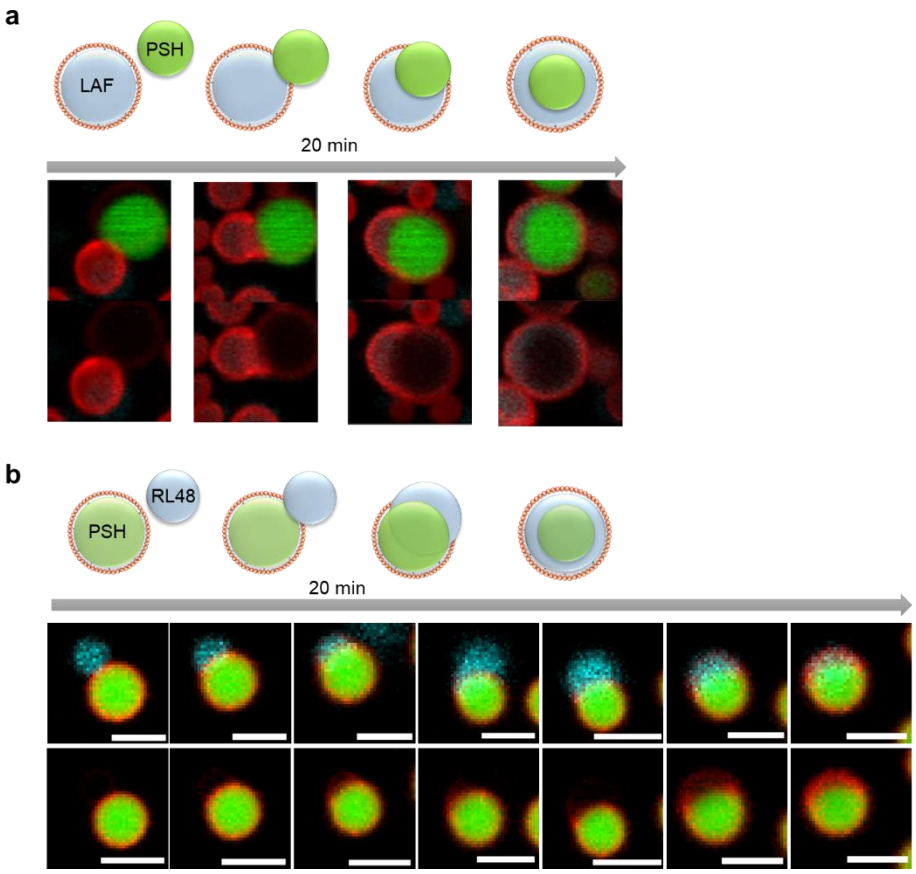

Figure S18. Schematics and confocal images of (a) PSH condensate (green) engulfing by a LAF protocell (red: lipid) or (b) RL48 condensate (cyan) engulfing by a PSH protocell (red: lipid). Scale bars 5 μm.

Table S1. Permeability enrichment indices (partition coefficient: inner mean intensity/outer mean intensity). S.D. (n>3).

- Figure 3

External materials	GUV	PSH	RL48
Calcein	0.09 ± 0.01	1.11 ± 0.07	0.94 ± 0.01
21 bp DNA	2.39 ± 0.89*	343.6 ± 35.82	440.19 ± 32.84
GFP	0.56 ± 0.19	0.86 ± 0.29	35.69 ± 1.45

*21 bp DNA was highly enriched around GUV surfaces, leading to slightly higher mean DNA signals inside GUV than outside.

- Figure S13

External materials	PSH	RL48 + PSH
360 bp DNA	33.26 ± 11.50	13.84 ± 7.44

- Figure S14

External materials	PSH	RL48	RL48 + PSH
PEG 5k	0.65 ± 0.04	0.74 ± 0.05	0.58 ± 0.02
Ft	7.87 ± 1.20	33.04 (n=1)	29.79 ± 14.85
mi3	72.05 ± 12.89	51.71 ± 21.48	28.55 ± 3.12
GFP	-	-	23.63 ± 1.32

- Figure S16c

External materials	RL48+ D7N-PSH
Calcein	0.60 ± 0.02
PEG 5k	0.69 ± 0.05
21 bp DNA	382.81 ± 39.80
360 bp DNA	39.99 ± 22.74
GFP	38.89 ± 1.78
WtF	28.46 ± 5.42
mi3	161.26 ± 38.55

Protein sequences

Protein	Amino acid sequence
GFP	MKGEELFTGVVPILVELDGDVNGHEFSVRGEGEGDATIGKLTLKFICTTGKLPVPWPTL VTTLTYGVQCFSRYPDHMKRHDFFKSAMPEGYVQERTISFKDDGKYKTRAVVKFEGDT LVNRIELKGTDFKEDGNILGHKLEYNFNSHDVYITADKQENGIKAEFTVRHNVEDGSVQ LADHYQQNTPIGDGPVLLPDNHYLSTQTVLSKDPNEKRDHMVL HEYVNAAGITLEHHHHHH
PRM-SH3-HIS (PSH)	MKKKKTAPTPPKRSGGSDLNMPAYVKFNYMAEREDELSLIKGTKVIVMEKSSDGWWR GSYNGQVGWFPSNYVTEEGDSPLGSENLYFQGLEHHHHHH
PRM-SH3-RL48-HIS (RL48)	MKKKKTAPTPPKRSGGSDLNMPAYVKFNYMAEREDELSLIKGTKVIVMEKSSDGWWR GSYNGQVGWFPSNYVTEEGDSPLGSEAAAKEAAAKEAAAKEAAAKEAAAKEAAAKEA AAKEAAAKGSGSLEHHHHHH
GFP-PRM-SH3-HIS	MKGEELFTGVVPILVELDGDVNGHEFSVRGEGEGDATIGKLTLKFICTTGKLPVPWPTL VTTLTYGVQCFSRYPDHMKRHDFFKSAMPEGYVQERTISFKDDGKYKTRAVVKFEGDT LVNRIELKGTDFKEDGNILGHKLEYNFNSHDVYITADKQENGIKAEFTVRHNVEDGSVQ LADHYQQNTPIGDGPVLLPDNHYLSTQTVLSKDPNEKRDHMVLHEYVNAAGITGSKKK KTAPTPPKRSGGSDLNMPAYVKFNYMAEREDELSLIKGTKVIVMEKSSDGWWRGSYN GQVGWFPSNYVTEEGDSPLGSENLYFQGLEHHHHHH
D7N-PSH	MAHIVMVNAYKPTKGGSKKKKTAPTPPKRSGGSDLNMPAYVKFNYMAEREDELSLIKG TKVIVMEKSSDGWWRGSYNGQVGWFPSNYVTEEGDSPLGSENLYFQGLEHHHHHH
Z_E-PSH	MLEIEAAALEQENTALETEVAELEQEVQRLENIVSQYRTRYGPLGSKKKKTAPTPPKRS GGSDLNMPAYVKFNYMAEREDELSLIKGTKVIVMEKSSDGWWRGSYNGQVGWFPSN YVTEEGDSPLGSENLYFQGLEHHHHHH
SC-GFP	MKGEELFTGVVPILVELDGDVNGHKFSVRGEGEGDATIGKLTLKFICTTGKLPVPWPTL VTTLTYGVQCFSRYPKHMKRHDFFKSAMPEGYVQERTISFKDDGKYKTRAVVKFEGDT LVNRIELKGTDFKEDGNILGHKLEYNFNSHNVYITADKQKNGIKANFTVRHNVEDGSVQ LADHYQQNTPIGDGPVLLPDNHYLSTQTVLSKDPNEKRDHMVLHEYVNAAGITEFGAM VDTLSGLSSEQGQSGDMTIEEDSATHIKFSKRDEDGKELAGATMELRDSSGKTISTWIS DGQVKDFYLYPGKYTFVETAAPDGYEVATAITFTVNEQGQVTVNGKATKGDAHILEHHH HHH
Z_R-GFP	MKGSNTALRTRVAELRQRVQRLRNEVSQYETRYGPLGGGSGGGTGGGSGGGEFMV SKGEELFTGVVPILVELDGDVNGHKFSVSGEGEGDATYGKLTLKFICTTGKLPVPWPTL VTTLTYGVQCFSRYPDHMKQHDFFKSAMPEGYVQERTIFFKDDGNYKTRAEVKFEGD TLVNRIELKGIDFKEDGNILGHKLEYNYNSHNVYIMADKQKNGIKVNFKIRHNIEDGSVQL ADHYQQNTPIGDGPVLLPDNHYLSTQSALSKDPNEKRDHMVLLEFVTAAGITLGMDEL YKLEHHHHHH
SC-mCherry	MGSSHHHHHHSSGLVPRGSMGAMVDTLSGLSSEQGQSGDMTIEEDSATHIKFSKRDE DGKELAGATMELRDSSGKTISTWISDGQVKDFYLYPGKYTFVETAAPDGYEVATAITFTV NEQGQVTVNGKATKGDAHIGSMVSKGEEDNMAIIKEFMRFKVHMEGSVNGHEFEIEG EGEGRPYEGTQTAKLKVTKGGPLPFAWDILSPQFMYGSKAYVKHPADIPDYLKLSFPE GFKWERVMNFEDGGVVTVTQDSSLQDGEFIYKVKLRGTNFPSDGPVMQKKTMGWEA SSERMYPEDGALKGEIKQRLKLKDGGHYDAEVKTTYKAKKPVQLPGAYNVNIKLDITSH NEDYTIVEQYERAEGRHSTGGMDELYK

DNA Sequences

DNA	DNA sequence
21 bp DNA	TTAAAGCAGCCATTGGAACGG-FAM
Cy5-360 bp DNA	Cy5- ACCACCGGTGCGATGGTTGACACCCTGTCTGGTCTGTCTTCTGAACA GGGTCAGTCTGGTGACATGACCATCGAAGAAGACTCTGCG ACCCACATCAAATTCTCTAAACGTGACGAAGACGGTAAAG AACTGGCGGGTGCGACGATGGAACTGCGTGACTCTTCTGG TAAAACCATCTCTACCTGGATCTCTGACGGTCAGGTTAAA GACTTCTACCTGTACCCGGGTAAATACACCTTCGTTGAAAC CGCGGCGCCGGACGGTTACGAAGTTGCGACCGCGATCACC TTCACCGTTAACGAACAGGGTCAGGTTACCGTTAACGGTA AAGCGACC AAAGGTGACG CGCACATC GGATCC

Experimental Methods

Materials. 1,2-dioleoyl-sn-glycero-3-phosphocholine (DOPC), 1,2-dioleoyl-sn-glycero-3-[(N-(5-amino-1-carboxypentyl)iminodiacetic acid)succinyl] (nickel salt) (DGS-NTA(Ni)), and 1,2-dipalmitoyl-sn-glycero-3-phosphoethanolamine-N-(lissamine rhodamine B sulfonyl) (ammonium salt) (Liss Rhod PE) were purchased from Avanti polar lipids. Calcein and octyl glucoside were purchased from Sigma-Aldrich. mPEG-FITC 5k was purchased from Creative PEGWorks. 21 bp DNA (single strand, double strand) and a Cy5-tagged primer for 360 bp DNA preparation were synthesized from Genotech. Transmission Electron Microscopy grids (Carbon type-B, 200 mesh, copper) were purchased from TED PELLA, INC.

Protein expression. Genes were cloned into the pET-21a expression vector (EMD Biosciences), and the plasmids were transformed to Escherichia coli BL21 (DE3) for protein expression. The transformed cells were grown at 37 °C until OD600 reaches 0.8 and induced with 1 mM IPTG followed by incubation for 18 h at 20 °C. The induced cells were collected by centrifugation for 5 min at 6000 rpm and washed once using PBS. Harvested cells were lysed by sonication in an equilibration buffer (500 mM NaCl and 50 mM Tris pH 8.0). Lysed cells were centrifuged at 12000 rpm for 15 min, and His-tagged proteins were purified using Ni-IDA columns (BioProgen). Purified proteins were dialyzed into PBS at 4 °C, and concentration was determined by measuring A280. Ferritin, mi3, and LAF were prepared as previously reported.[1-3]

Fluorescent dye labeling of proteins. Proteins were labeled with the Cy5 N-hydroxysuccinimide (NHS) ester (Lumiprobe). Protein samples were mixed with the dye in a 10:1 protein-to-dye ratio and incubated for 1 h at RT. Dye-conjugated proteins were separated using PD-10 desalting columns (SephadexTM G-25 M, GE Healthcare).

GUV preparation. Giant Unilamellar vesicle (GUV) was produced based on the published protocel.[4] Briefly, 2 μL of a 2 mM lipid mix (94.5 mol% DOPC, 5 mol% DGS-NTA (Ni), 0.5 mol% Liss Rhod PE) dissolved in chloroform was spread on inidium-tin-oxide (ITO) coated glass (resistance ~ 10 Ω-sq−1) slides, followed by overnight drying. Two ITO glass slides were spaced using a rubber ring and electectroformed with a sinusoidal voltage of 1 kHz with an amplitude of 2.5 V root mean square (RMS) for 3 h at 45 °C in PBS.

Lipid-coated protein condensate preparation. Protein (PSH) consendates were prepared by adding 100 μM $NiCl_2$ to 100 μM PSH (final 50 μL) to induce phase separation. After 10 min (or indicated time) incubation, 10 μL of 2.5 mM lipid mix (94.5 mol% DOPC, 5 mol% DOGS-Ni NTA, 0.5 mol% DPPE-Lissamine Rhodamine B in 2% OG solution) was added to condensates (final protein:lipid concentration = 1:5 or to indicated ratios), where a final OG concentration was controlled to 0.67%. Following lipid-condensate binding for 10 min, the solution is diluted with 1xPBS to obtain a 0.2% final OG concentration. The resulting lipid-coated condensates were centrifuged at 3500 rpm for 5 min,

followed by resuspension to 1xPBS. For RL48 condensate formation, reaction tubes were blocked with BSA to prevent condensate attachment to tube surfaces. Protein condensates of RL48 or RL48 with indicated amounts of PSH proteins (PSH, D7N-PSH, or Z_E-PSH) were prepared by adding 800 μM $NiCl_2$ to 300 μM RL48 proteins. Phase separation was conducted for 30 min before lipid coating. Again, 10 μL of 2.5 mM lipid mix was mixted with 50 μL of the RL48 condensate solution. For LAF droplet condensate formation, 100 μM $NiCl_2$ was treated to 80 μM LAF, followed by 10 min incubation before lipid coating (10 μL of 2.5 mM lipid mix to 50 μL of the condensate solution).

Permeability and uptake assays. For permeability tests, protocells were prepared and isolated by centrifugation, and 10 μM of external proteins were treated to these protocells. For selective uptake tests, 0.1 μM of external proteins were treated to these protocells. The protein concentrations of external proteins that were recruited into protocells were estimated based on GFP intensity/concentration calibration curves.

Confocal imaging and FRAP analysis. Fluorescence confocal images were obtained in BSA-coated flat bottmed 96-well plates (SPL) with LSM 800 laser scanning confocal microscope (Carl Zeiss) using 63x/1.40 NA plan-apochromatic oil-imersion objetive lens. For GUV observation, a slide glass was coated with streptavidin followed by BSA coating. For fluorescence recovery after photobleaching (FRAP), lipid-coated condensates were observed in a μ-slide (18 well – flat uncoated) (Ibidi). Bleaching was conducted with a 488 nm (5% laser power) or 561 nm (40%) laser for GFP-fused protein or Liss Rhod PE, respectively. Time lapse images were taken in 5 sec interval. Intensities of region of interest (bleached region), background and reference regions were measured and processed using Origin. Recovery curves were obtained basically with $(I_{ROI} - I_{BG})/(I_{REF} - I_{BG})$ (I_{ROI}: Intensity of region of interest, I_{BG}: Intensity of background, I_{REF}: Intensity of reference region) and revised to $[(I_{ROI} - I_{BG})/(I_{REF} - I_{BG})]/ [(I_{ROI} - I_{BG})/(I_{REF} - I_{BG})]_{t=0}$ as previously describe.[5]

TEM imaging. Lipid-coated condensate samples were loaded onto a carbon grid for 10 sec and soaked using a filter paper. Liposomal giant unilamellar vesicles (GUV) were loaded onto a carbon grid for 30 sec and stainined for 30 sec using 2% uranyl acetate solution, followed by soaking using a filter paper. 200 kV Transmission Electron Microscope (Tecnai F20) (FEI Company) was used for observation.

1. B. Ahn, S. G. Lee, H. R. Yoon, J. M. Lee, H. J. Oh, H. M. Kim and Y. Jung, *Angew. Chem. Int. Ed.*, 2018, **57**, 2909-2913.

2. Y. Hsia, J. B. Bale, S. Gonen, D. Shi, W. Sheffler, K. K. Fong, U. Nattermann, C. Xu, P.-S. Huang, R. Ravichandran, S. Yi, T. N. Davis, T. Gonen, N. P. King and D. Baker, *Nature*, 2016, **535**, 136-139.
3. Y. Jo and Y. Jung, *Chem. Sci.*, 2019, **11**, 1269-1275.
4. M. I. Angelova and D. S. Dimitrov, *Faraday Discussions of the Chemical Society*, 1986, **81**, 303-311.
5. K. Hong, D. Song and Y. Jung, *Nat. Commun.*, 2020, **11**, 5554.